# Optimization of Trap Locations for Narrow Capture Problems

Alexei Cheviakov and Michael Ward

**Abstract** The determination of the mean first passage time (MFPT) for a Brownian particle in a domain that contains a collection of small absorbing traps in its interior is a narrow capture problem with many biophysical applications. The average MFPT is the expected capture time assuming a uniform distribution of starting points for the random walk. We survey some results for determining the spatial locations of the traps that minimize the average MFPT for certain 2-D and 3-D domains. In the limit of small trap radii, the optimization of the average MFPT over the trap locations can be reduced to the problem of seeking global minima of a discrete energy for an interacting particle system that is encoded by the Neumann Green's matrix. Open problems for the optimization of the average MFPT are discussed.

## 1 Introduction

Narrow capture problems arise naturally in models of diffusive transport in cellular biology owing to the highly heterogeneous spatial environment that diffusing signaling molecules typically encounter before reaching a specific target site to initiate some biological function [1–4]. Modeling these diffusing signaling molecules as Brownian particles, a narrow capture problem involves calculating the mean time, and other related averaged quantities, that such a particle takes in order to reach a small target when it is confined within a multi-dimensional domain. More generally, an overview of results for a wide variety of first passage-problems and their applications are given in [5] and [6].

Alexei Cheviakov
Dept. of Mathematics and Statistics, U. of Saskatchewan, Saskatoon, SK, Canada, S7N 5E6 e-mail: shevyakov@math.usask.ca

Michael J. Ward
Dept. of Mathematics, University of British Columbia, Vancouver, BC, Canada, V6T 1Z2 e-mail: ward@math.ubc.ca

In this article, we exploit the connection between mean first passage time problems and PDE problems that have origins in electrostatics. In a bounded domain $\Omega$ containing $N$ small traps, the mean first passage time $u(\mathbf{x})$ for a narrow capture problem is the solution to the singularly perturbed PDE

$$\begin{aligned} D\,\Delta u = -1\,, \quad \mathbf{x} \in \bar{\Omega}\,; \qquad & \bar{\Omega} \equiv \Omega \setminus \cup_{j=1}^{N} \Omega_{\varepsilon j}\,, \\ \partial_n u = 0\,, \quad \mathbf{x} \in \partial\Omega\,; \qquad & u = 0\,, \quad \mathbf{x} \in \partial\Omega_{\varepsilon j}\,, \quad j = 1, \ldots, N\,. \end{aligned} \tag{1}$$

The small traps $\Omega_{\varepsilon j}$, each of radius $\mathcal{O}(\varepsilon) \ll 1$, are centered at locations $\mathbf{x}_1, \ldots, \mathbf{x}_N$ within $\Omega$. We assume that the traps are well-separated in the sense that $|\mathbf{x}_i - \mathbf{x}_j| = \mathcal{O}(1)$ for $i \neq j$ and that $\mathrm{dist}(\partial\Omega, \mathbf{x}_j) = \mathcal{O}(1)$ as $\varepsilon \to 0$. The prototypical case in 2-D and 3-D is where the traps are all either disks or spheres, respectively, of a common radius $\varepsilon$. The average MFPT $\overline{u}$, which assumes that the starting point for Brownian motion is uniformly distributed over the domain, is the spatial average

$$\overline{u} \equiv \frac{1}{|\bar{\Omega}|} \int_{\bar{\Omega}} u \, \mathrm{d}\mathbf{x}\,. \tag{2}$$

Our goal for a fixed $N$ is to identify the locations $\mathbf{x}_1, \ldots, \mathbf{x}_N$ of the traps that minimizes $\overline{u}$. Such an optimal trap configuration is the one that most rapidly captures, on average, a Brownian particle when the initial starting point for the random walk is uniformly distributed in the domain.

With regards to full numerical PDE simulations, the identification of optimal trap configurations for (1) is a challenging shape optimization problem since the trap locations must be adjusted and the PDE re-meshed and re-solved at each iterate of an optimization procedure. For an arbitrary 2-D domain with a collection of circular traps of small radius $\varepsilon \ll 1$, a **closest-point method (CPM)** coupled to a particle-swarm optimizer was developed in [7] to compute optimal trap patterns.

From the viewpoint of asymptotic analysis, in the limit $\varepsilon \to 0$ strong localized perturbation theory [8,9] can be used to derive an approximation $\overline{u}_0$ for the average MFPT. For a survey of strong localized perturbation for MFPT problems and in other contexts see [10]. In the limit $\varepsilon \to 0$ for a 2-D or 3-D domain, we obtain

$$\overline{u} \sim \overline{u}_0 + \mathcal{O}(\varepsilon^m)\,, \qquad \overline{u}_0 \equiv \frac{1}{|\Omega|} \int_{\Omega} u_0 \, \mathrm{d}\mathbf{x}\,, \tag{3}$$

where $m = 2$ (2-D) or $m = 3$ (3-D). Here, for $\varepsilon \to 0$, $u_0$ is the outer approximation for the solution to (1) when the traps are replaced by effective point singularities at the "particles" $\mathbf{x}_j \in \Omega$ for $j = 1, \ldots, N$. In this limiting problem, traps of different shapes are encoded by their logarithmic capacitances or capacitances in a 2-D or 3-D setting, respectively. These trap-shape dependent terms can be calculated separately from certain **local problems** for Laplace's equation that are valid in the near-field region of a trap. The explicit solution to this limiting system in terms of the Neumann Green's function determines a discrete energy for our effective "interacting-particle" system that is defined in terms of the Neumann Green's matrix, which depends on the trap locations. By applying particle-swarm optimization software to this discrete

energy the asymptotic prediction for optimal trap configurations can be readily computed for moderately small $N$. However, as is typically the case with optimizing the discrete energy associated with other interacting-particle systems, as $N$ increases it becomes increasingly more challenging to numerically identify globally optimal trap patterns owing to the existence of many local minima [12].

As shown in Appendix C of [11] the problem of identifying optimal trap configurations that minimize the average MFPT is closely related to a classical problem in spectral theory of identifying trap locations that maximize the fundamental Neumann eigenvalue for the Laplacian in the domain with traps. For this class of eigenvalue problem, optimal trap locations have been analyzed in [13–19].

The outline of this brief survey is as follows. In §2 and §3 we highlight some previous results obtained for certain specific 2-D and 3-D domains, respectively. For a 2-D or 3-D domain with small traps, in §4 we relate the problem of minimizing the average MFPT to the spectral problem of maximizing the fundamental Neumann eigenvalue for the Laplacian. In §5 we discuss some related narrow capture and escape problems, and we suggest a few open problems.

## 2 2-D Domains

A hybrid asymptotic-numerical method was implemented for (1) to identify optimal trap configurations that minimize the average MFPT for disk-shaped domains [17], for near-disk domains [7], and for elliptical-shaped domains [11, 20]. For a class of dumbbell-shaped domains, the optimal location of a single trap has been identified in [17]. A full numerical approach to compute optimal trap configurations for (1) using the closest point methodology (CPM) of [21] was developed in [7]. In this way, approximate optimization results obtained from the hybrid asymptotic-numerical theory, which is based on the assumption of small trap radii, were validated.

In a 2-D domain, strong localized perturbation theory can be applied to (1) in the limit of small trap radii to derive a linear algebraic system (LAS) that determines the average MFPT in terms of the spatial locations of $N$ traps. In this asymptotic limit, the spatial interaction between the traps is mediated by the Neumann Green's matrix, which is defined in terms of the Neumann Green's function for the domain.

We now highlight the derivation of this LAS. Under the assumption that the traps $\Omega_{\varepsilon j}$ have a common shape, the outer problem $u_0$ satisfies [11, 22]

$$\begin{aligned} &D\Delta u_0 = -1\,, \quad \mathbf{x} \in \Omega \setminus \{\mathbf{x}_1, \ldots, \mathbf{x}_N\}\,; \quad \partial_n u_0 = 0\,, \ \ \mathbf{x} \in \partial\Omega\,; \\ &u_0 \sim A_j \log|\mathbf{x} - \mathbf{x}_j| + A_j/\nu \quad \text{as} \quad \mathbf{x} \to \mathbf{x}_j\,, \qquad j = 1, \ldots, N\,, \end{aligned} \tag{4}$$

where $\nu \equiv -1/\log(\varepsilon d)$ and $A_j$ for $j = 1, \ldots, N$ are to be determined. Here $d$ is the logarithmic capacitance associated with the assumed common trap shape, which is independent of the orientation of the traps in the domain. It is defined by the solution to the following local problem near a trap formulated in terms of $\mathbf{y} = \varepsilon^{-1}(\mathbf{x} - \mathbf{x}_j)$:

$$\begin{aligned} &\Delta_{\mathbf{y}} v = 0\,, \quad \mathbf{y} \notin \Omega_j\,; \quad v = 0\,, \quad \mathbf{y} \in \partial\Omega_j\,, \\ &\quad v \sim \log|\mathbf{y}| - \log d + \mathcal{O}(|\mathbf{y}|^{-1})\,, \quad \text{as} \quad |\mathbf{y}| \to \infty\,, \end{aligned} \tag{5}$$

where $\Omega_j = \Omega_{\varepsilon j}/\varepsilon$. If $\Omega_{\varepsilon j}$ are disks of a common radius $\varepsilon$ then $\Omega_j$ is the unit disk and $d = 1$ from (5). Table 1 of [22] gives $d$ for traps of other shapes.

The solution to (4) is

$$u_0 = -2\pi \sum_{k=1}^{N} A_k G(\mathbf{x};\mathbf{x}_k) + \overline{u}_0\,, \qquad \text{where} \qquad \overline{u}_0 = \frac{1}{|\Omega|}\int_\Omega u_0\,d\mathbf{x}\,. \tag{6}$$

Here $\overline{u}_0$ is the approximation to the average MFPT (see (3)) and $G(\mathbf{x};\mathbf{x}_j)$ is the unique Neumann Green's function satisfying

$$\begin{aligned} &\Delta G = \frac{1}{|\Omega|} - \delta(\mathbf{x}-\mathbf{x}_j)\,, \quad \mathbf{x}\in\Omega\,; \quad \partial_n G = 0\,, \ \ \mathbf{x}\in\partial\Omega\,; \quad \int_\Omega G\,d\mathbf{x} = 0\,, \\ &G \sim -\frac{1}{2\pi}\log|\mathbf{x}-\mathbf{x}_j| + R_j + \nabla_{\mathbf{x}} R_j\cdot(\mathbf{x}-\mathbf{x}_j) + \cdots\,, \quad \text{as} \quad \mathbf{x}\to\mathbf{x}_j\,. \end{aligned} \tag{7}$$

Moreover, $R_j \equiv R(\mathbf{x}_j)$ is the regular part of the Green's function at $\mathbf{x} = \mathbf{x}_j$. By enforcing that $u_0$ in (6) satisfies the singularity conditions in (4), we obtain that $\overline{u}_0$ is given in terms of a LAS and a discrete energy $q(\mathbf{x}_1,\ldots,\mathbf{x}_N)$ defined by

$$\begin{aligned} &\overline{u}_0 = \frac{|\Omega|}{2\pi D\nu N} + \frac{2\pi}{N} q(\mathbf{x}_1,\ldots,\mathbf{x}_N)\,, \\ &\text{where} \quad q \equiv \mathbf{e}^T\mathcal{G}\mathcal{A} \quad \text{and} \quad \Big[I + 2\pi\nu(I-E)\mathcal{G}\Big]\mathcal{A} = \frac{|\Omega|}{2\pi DN}\mathbf{e}\,. \end{aligned} \tag{8}$$

Here $E \equiv \mathbf{e}\mathbf{e}^T/N$, $\mathbf{e} \equiv (1,\ldots,1)^T$, $\mathcal{A} \equiv (A_1,\ldots,A_N)^T$, $I$ is the identity matrix, and $\nu \equiv -1/\log(\varepsilon d)$. The $N\times N$ symmetric Neumann Green's matrix $\mathcal{G}$, which depends on the trap locations $\mathbf{x}_1,\ldots,\mathbf{x}_N$, has matrix entries

$$(\mathcal{G})_{jj} = R_j\,, \quad \text{and} \quad (\mathcal{G})_{ij} = (\mathcal{G})_{ji} = G(\mathbf{x}_i;\mathbf{x}_j) \ \text{ for } \ i\neq j\,. \tag{9}$$

For $\nu \ll 1$, for which we can estimate $\mathcal{A} \sim |\Omega|\mathbf{e}/(2\pi DN) + \mathcal{O}(\nu)$, (8) yields the following two-term approximation for $\overline{u}_0$ in terms of $\nu \ll 1$:

$$\overline{u}_0 = \tilde{u}_0 + \mathcal{O}(\nu^2)\,, \quad \text{with} \quad \tilde{u}_0 \equiv \frac{|\Omega|}{2\pi D\nu N}\left[1 + \frac{2\pi\nu}{N}p(\mathbf{x}_1,\ldots,\mathbf{x}_N)\right]\,, \quad p \equiv \mathbf{e}^T\mathcal{G}\mathbf{e}\,. \tag{10}$$

When $G(\mathbf{x};\mathbf{x}_j)$ is known analytically as either an explicit formula or as a rapidly converging infinite series, the optimal trap locations in the limit $\varepsilon\to 0$ can be calculated numerically by applying particle swarm optimization schemes [23–25] to the LAS (8) to minimize $q$ and hence $\overline{u}_0$. Domains for which $G$ is readily available are disks, rectangles (see §4.2 of [26] and §3.2 of [27]), and ellipses. In §2.1 and §2.2 we highlight some results for optimal trap patterns for the disk and the ellipse. For a spatially periodic arrangement of traps, in §2.3 we discuss results from [28]

for the optimization of $\overline{u}_0$ over the class of Bravais lattices with a fixed area of the primitive cell.

## 2.1 The Unit Disk

For the unit disk, the Neumann Green's function and its regular part for (7) are [17]

$$G(\mathbf{x};\mathbf{x}_j) = -\frac{1}{2\pi}\log|\mathbf{x}-\mathbf{x}_j| - \frac{1}{4\pi}\log\left(|\mathbf{x}|^2|\mathbf{x}_j|^2 + 1 - 2\mathbf{x}\cdot\mathbf{x}_j\right) + \frac{|\mathbf{x}|^2}{4\pi} + \frac{|\mathbf{x}_j|^2}{4\pi} - \frac{3}{8\pi}\,,$$
$$R(\mathbf{x}_j) = -\frac{1}{2\pi}\log\left(1-|\mathbf{x}_j|^2\right) + \frac{|\mathbf{x}_j|^2}{2\pi} - \frac{3}{8\pi}\,. \tag{11}$$

In this way, the Neumann Green's matrix $\mathcal{G}$ in (8) and (10) is readily evaluated.

In [17] a restricted optimization of the discrete energy $p(\mathbf{x}_1,\ldots,\mathbf{x}_N)$ for $\tilde{u}_0$ in (10) was undertaken for $2 \le N \le 25$ where the traps were forced to lie on concentric rings about the origin, with possibly a center trap. For such two- and three-ring patterns analytical expressions for $p$ were derived in [17] in terms of the ring radii and the number of traps on each ring. The results of this restricted optimization process for $p$ for $6 \le N \le 25$ are shown in Fig. 1 (see also Table 2 of [17]). With the restricted optimal values of $p$ determined in this way, the two-term approximation $\tilde{u}_0$ in (10) can be estimated for a given $\varepsilon$ and $D$.

In [20] the results of the restricted optimization in [17] were compared with corresponding results computed by optimizing $\overline{u}_0$ in the LSA (8) by using a particle swarm optimizer on $q$ in (8) over the $2N$ variables $\mathbf{x}_j = (x_j, y_j)$ with $j = 1,\ldots,N$ and $|\mathbf{x}_j| < 1$ (see [20] for details). In Fig. 2 we show a reasonably close comparison between the optimal $\tilde{u}_0$ and $\overline{u}_0$ for $6 \le N \le 25$ when $\varepsilon = 0.05$ and $D = 1$. In [20] it was shown that as $N$ increases the optimal trap configuration begins to deviate significantly from a ring-type structure (see Figures 4a)–7a) of [20]).

Finally, we show that when $N$ traps are equally-spaced on one ring of radius $r$ concentric within the unit disk, the approximate result $\tilde{u}_0$ in (10) is an exact solution to the LSA (8). For such a ring pattern, the Neumann Green's matrix is cyclic and symmetric and has the eigenpair (see Principal Result 4.3 of [17])

$$\mathcal{G}\mathbf{e} = \sigma\mathbf{e}\,, \quad \sigma = \sigma(r) \equiv \frac{1}{2\pi}\left(-\log\left(Nr^{N-1}\right) - \log\left(1-r^{2N}\right) + r^2 N - \frac{3N}{4}\right)\,. \tag{12}$$

Since $(I-E)\mathbf{e} = 0$, the solution to (8) for $\mathcal{A}$ is $\mathcal{A} = |\Omega|\mathbf{e}/(2\pi DN)$, so that

$$\overline{u}_0 = \tilde{u}_0 = \frac{|\Omega|}{2\pi DN\nu}\left(1 + 2\pi\sigma\nu\right)\,. \tag{13}$$

The optimal ring radius $r_c$ is found by setting $d\sigma/dr = 0$ and solving for $r = r_c$. For $D = 1$ and $\varepsilon = 0.003$, and for $2 \le N \le 10$, in Fig. 3 we show a very close

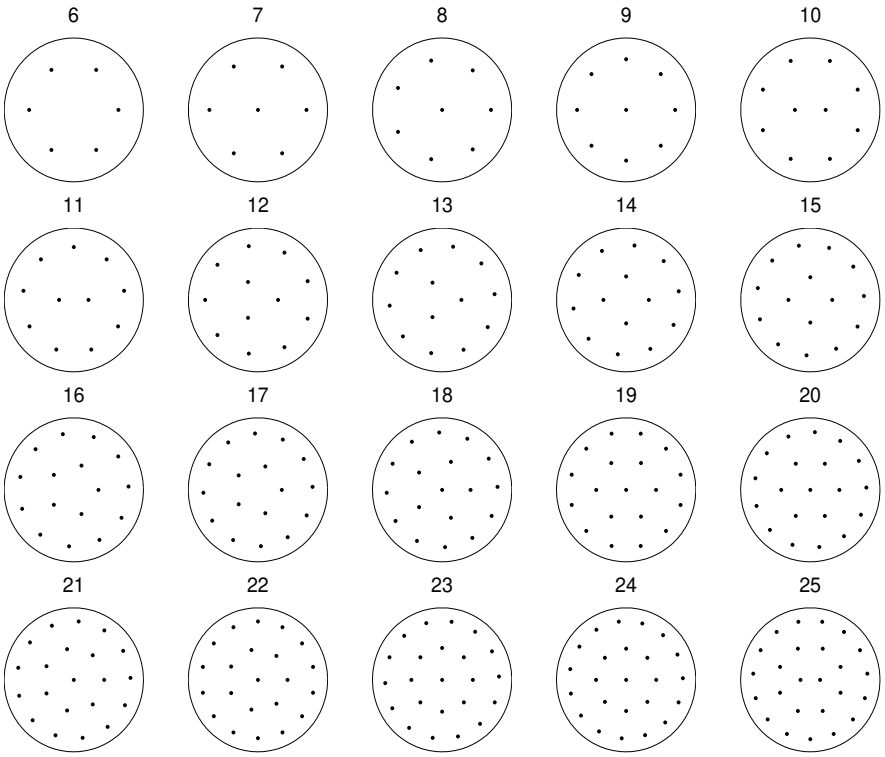


Fig. 1: The optimum configurations for $N = 6$ to $N = 25$ traps for the discrete energy $p$ in (10) for the class of two-ring and three-ring patterns, with possibly a centre trap.

comparison between $r_c$ obtained from (13) with that computed by the CPM from the full PDE (1) for the restricted optimization problem where $N$ equally-spaced traps are restricted to one ring that is concentric within the unit disk (see Fig. 4 of [7]).

## 2.2 The Ellipse

A new rapidly converging infinite series representation for the Neumann Green's function $G(\mathbf{x};\mathbf{x}_0)$ and its regular part $R(\mathbf{x}_0)$ for an elliptical-shaped domain $\Omega \equiv \{\mathbf{x} = (x, y) \,|\, x^2/a^2 + y^2/b^2 \leq 1\}$ with $a > b$ was derived in §5 of [11].

In the analysis of [11], the ellipse was first mapped to a rectangular domain $0 \leq \xi \leq \xi_b$ and $0 \leq \eta \leq 2\pi$ using the elliptical coordinates $(\xi, \eta)$ defined by

$$x = f \cosh\xi \cos\eta\,, \quad y = f \sinh\xi \sin\eta\,, \quad f = \sqrt{a^2 - b^2}\,, \tag{14}$$

| $N$ | $\tilde{u}_0$ | $\overline{u}_0$ |
|---|---|---|
| 6 | 0.11648 | 0.11648 |
| 7 | 0.09299 | 0.09297 |
| 8 | 0.07660 | 0.07660 |
| 9 | 0.06518 | 0.06512 |
| 10 | 0.05653 | 0.05624 |
| 11 | 0.04920 | 0.04900 |
| 12 | 0.04291 | 0.04278 |
| 13 | 0.03805 | 0.03796 |
| 14 | 0.03380 | 0.03375 |
| 15 | 0.03042 | 0.03038 |
| 16 | 0.02747 | 0.02745 |
| 17 | 0.02502 | 0.02499 |
| 18 | 0.02286 | 0.02280 |
| 19 | 0.02078 | 0.02076 |
| 20 | 0.01909 | 0.01907 |
| 21 | 0.01756 | 0.01755 |
| 22 | 0.01626 | 0.01624 |
| 23 | 0.01512 | 0.01510 |
| 24 | 0.01411 | 0.01403 |
| 25 | 0.01314 | 0.01307 |

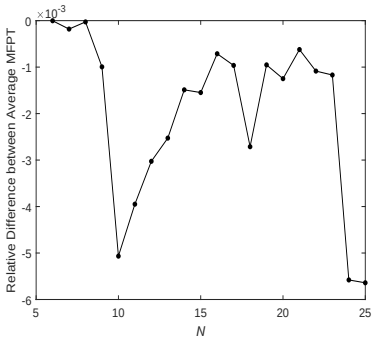


Fig. 2: Left: The optimal average MFPT $\tilde{u}_0$ in the unit disk for a restricted optimization with traps equally spaced on rings (see [17]) is compared with $\overline{u}_0$ from the LSA (8) for optimal trap locations. Right: The relative difference $(\overline{u}_0 - \tilde{u}_0)/\tilde{u}_0$ versus $N$.

| $N$ | $\tilde{u}_0$ | $\overline{u}$ (CPM) |
|---|---|---|
| 2 | 0.4536 | 0.4533 |
| 3 | 0.5517 | 0.5480 |
| 4 | 0.5985 | 0.5987 |
| 5 | 0.6251 | 0.6275 |
| 6 | 0.6417 | 0.6411 |
| 7 | 0.6527 | 0.6467 |
| 8 | 0.6604 | 0.6609 |
| 9 | 0.6662 | 0.6689 |
| 10 | 0.6706 | 0.6708 |

(a) Optimal ring radius $r_c$ for $N$ traps.

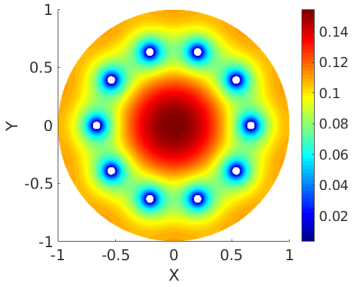


(b) MFPT for the optimal 10 trap ring.

Fig. 3: The optimal ring radius $r_c$ for $N$ circular traps of radius $\varepsilon = 0.003$ that are equally-spaced on a ring concentric within the unit disk. Left: Comparison of asymptotic results obtained by minimizing (13) with full numerical results computed from the MFPT-PDE (1) by the CPM. Right: The optimal MFPT $u(\mathbf{x})$ in the unit disk computed from (1) from the CPM with $N = 10$ traps on a ring.

where

$$\xi_b = \tanh^{-1}\left(\frac{b}{a}\right) = -\frac{1}{2}\log\beta\,, \quad \text{with} \quad \beta \equiv \left(\frac{a-b}{a+b}\right). \tag{15}$$

For a given pair $(x, y)$, $(\xi, \eta)$ is determined by inverting the transformation (14) as

$$\xi = \frac{1}{2}\log\left(1 - 2s + 2\sqrt{s^2 - s}\right), \quad s \equiv \frac{-\mu - \sqrt{\mu^2 + 4f^2y^2}}{2f^2}, \quad \mu \equiv x^2 + y^2 - f^2\,,$$
$$\eta = \begin{cases} \eta_\star, & \text{if } x \geq 0\,,\ y \geq 0\,, \\ \pi - \eta_\star, & \text{if } x < 0\,,\ y \geq 0\,, \\ \pi + \eta_\star, & \text{if } x \leq 0\,,\ y < 0\,, \\ 2\pi - \eta_\star, & \text{if } x > 0\,,\ y < 0\,, \end{cases} \quad \text{with } \eta_\star \equiv \sin^{-1}\left[\left(\frac{-\mu + \sqrt{\mu^2 + 4f^2y^2}}{2f^2}\right)^{1/2}\right]. \tag{16}$$

In this way, the Dirac point at $\mathbf{x}_0 = (x_0, y_0)$ is mapped to $(\xi_0, \eta_0)$.

The analysis in §5 of [11] determined $G$ as

$$G(\mathbf{x};\mathbf{x}_0) = \frac{1}{4|\Omega|}\left(|\mathbf{x}|^2 + |\mathbf{x}_0|^2\right) - \frac{3}{16|\Omega|}(a^2+b^2) - \frac{1}{4\pi}\log\beta - \frac{1}{2\pi}\xi_> \\ - \frac{1}{2\pi}\sum_{n=0}^{\infty}\log\left(\prod_{j=1}^{8}|1 - \beta^{2n}z_j|\right), \quad \text{for} \quad \mathbf{x} \neq \mathbf{x}_0\,, \tag{17}$$

where $|\Omega| = \pi ab$, $\xi_> \equiv \max(\xi, \xi_0)$, and the complex constants $z_1, \ldots, z_8$ are defined in terms of $(\xi, \eta)$, $(\xi_0, \eta_0)$ and $\beta$ by

$$z_1 \equiv e^{-|\xi-\xi_0|+i(\eta-\eta_0)}, \quad z_2 \equiv \beta^2 e^{|\xi-\xi_0|+i(\eta-\eta_0)}, \quad z_3 \equiv \beta e^{-(\xi+\xi_0)+i(\eta-\eta_0)}, \\ z_4 \equiv \beta e^{\xi+\xi_0+i(\eta-\eta_0)}, \quad z_5 \equiv \beta^2 e^{\xi+\xi_0+i(\eta+\eta_0)}, \quad z_6 \equiv e^{-(\xi+\xi_0)+i(\eta+\eta_0)}, \\ z_7 \equiv \beta e^{|\xi-\xi_0|+i(\eta+\eta_0)}, \quad z_8 \equiv \beta e^{-|\xi-\xi_0|+i(\eta+\eta_0)}. \tag{18}$$

By letting $(\xi, \eta) \to (\xi_0, \eta_0)$, the regular part of the Neumann Green's function is

$$R(\mathbf{x}_0) = \frac{|\mathbf{x}_0|^2}{2|\Omega|} - \frac{3(a^2+b^2)}{16|\Omega|} + \frac{1}{2\pi}\log(a+b) + \frac{1}{4\pi}\log\left(\cosh^2\xi_0 - \cos^2\eta_0\right) \\ - \frac{\xi_0}{2\pi} - \frac{1}{2\pi}\sum_{n=1}^{\infty}\log(1-\beta^{2n}) - \frac{1}{2\pi}\sum_{n=0}^{\infty}\log\left(\prod_{j=2}^{8}|1-\beta^{2n}z_j^0|\right), \tag{19}$$

where $z_j^0$ for $j = 2, \ldots, 8$ are given by

$$z_2^0 = \beta^2, \quad z_3^0 = \beta e^{-2\xi_0}, \quad z_4^0 = \beta e^{2\xi_0}, \quad z_5^0 = \beta^2 e^{2\xi_0+2i\eta_0}, \\ z_6^0 = e^{-2\xi_0+2i\eta_0}, \quad z_7^0 = \beta e^{2i\eta_0}, \quad z_8^0 = \beta e^{2i\eta_0}. \tag{20}$$

By using (17) and (19), the Neumann Green's matrix $\mathcal{G}$ in (9), as needed in the LAS (8), is readily evaluated. As a result, a particle swarm optimization procedure

was used in [11] and [20] to identify how the optimal trap configurations depend on the aspect ratio of the ellipse when its area is fixed as $|\Omega| = \pi ab = \pi$. In the rapidly converging infinite series (17) and (19), the aspect ratio of the ellipse is determined by the parameter $\beta$, as defined in (15), which satisfies $0 \le \beta < 1$.

In particular, when $N = 4$, $\varepsilon = 0.05$ and $D = 1$ we show in Fig. 4 and Fig. 5 that four optimally located traps become colinear with the semi-major axis of the ellipse when the ellipse becomes sufficiently elongated (see Fig. 10 and 11 of [11]). From our numerical computations using (8) we find that this transition to colinearity occurs for an ellipse of area $\pi$ when $a = a_c \approx 1.7$. It is an open problem to calculate the critical threshold $a_c$ analytically.

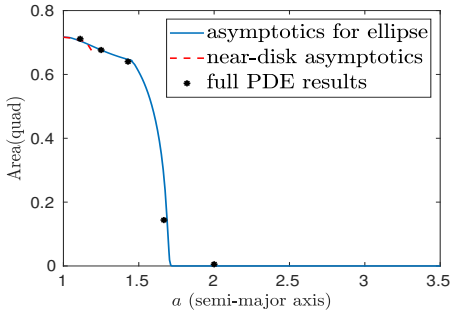


**Fig. 4** Area of the quadrilateral formed by four optimally located traps of a common radius $\varepsilon = 0.05$ with $D = 1$ in a deforming ellipse of area $\pi$ and semi-major axis $a$. The optimal traps become colinear as $a$ increases. Solid curve: results from (8). Discrete points: full numerical CPM results. Dashed line near $a = 1$: near-disk asymptotics of [11].

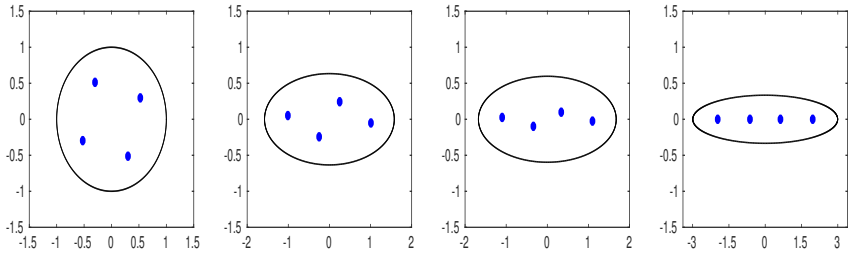

Fig. 5: Optimal four-trap patterns for $D = 1$ in a deforming ellipse of area $\pi$ with semi-major axis $a$ and a common trap radius $\varepsilon = 0.05$. Left: $a = b = 1$. Middle Left: $a = 1.577$, $b \approx 0.634$. Middle Right: $a = 1.675$, $b \approx 0.597$. Right: $a = 3.0$, $b = 1/3$. The optimal trap pattern is colinear along the major axis when $a > a_c \approx 1.75$.

As motivated by the colinear trap pattern in Fig. 5, for a long and thin ellipse where $a = 1/\delta \gg 1$, $b = \delta \ll 1$, and $|\Omega| = \pi$, we use thin domain asymptotics to formulate, as done in [11], a 1-D optimization problem for the optimal trap locations and the optimal average MFPT. Thin domain asymptotics for MFPT problems with a single trap have also been developed in a 2-D and 3-D setting in [29] and [30].

From Appendix A of [11], for the thin ellipse the MFPT is approximated as $u(x,y) \sim \delta^{-2} D^{-1} U_0(\delta x) + \mathcal{O}(\delta^{-1})$, where the 1-D profile $U_0(X)$ satisfies

$$\left[F(X)\, U_0'\right]' = -F(X)\,, \quad \text{on} \quad |X| \le 1\,, \quad \text{with} \quad F(X) \equiv \sqrt{1-X^2}\,, \tag{21}$$

where $X = \delta x$ and with $U_0$ and $U_0'$ bounded as $X \to \pm 1$. Assuming that $U_0(X) = U_0(-X)$, the average MFPT for the thin ellipse with $|\Omega| = \pi$ is estimated as

$$\overline{u}_0 \sim \frac{1}{\pi} \int_{-1/\delta}^{1/\delta} \int_{-\delta\sqrt{1-\delta^2 x^2}}^{\delta\sqrt{1-\delta^2 x^2}} u\, dx dy \sim \frac{4}{D\pi\delta^2} \int_0^1 F(X)\, U_0(X)\, dX\,, \tag{22}$$

where $b = \delta \ll 1$. For the approximating BVP (21), the colinear circular traps of a common radius $\varepsilon$ centered on the semi-major axis are approximated by zero point constraints for $U_0$ at locations on the interval $|X| \le 1$. Therefore, (21) is a multi-point BVP, whose solution depends on the locations of the zero point constraints. The optimal trap locations and optimal average MFPT are estimated by minimizing the 1-D integral (22) for $\overline{u}_0$ with respect to the locations of these point constraints.

Following §4.2 of [11], we illustrate this approach for $N = 4$ colinear traps in a thin ellipse. We assume that two optimal traps are located on either side of the origin and that $U_0(X) = U_0(-X)$. By symmetry, we first solve (21) with $U_0'(0) = 0$, $U_0(d_1) = 0$, and $U_0(d_2) = 0$, where $0 < d_1 < d_2$, to obtain

$$U_0(X) = -\frac{1}{4}\left[\left(\sin^{-1} X\right)^2 + X^2\right] - \frac{1}{4}\begin{cases} \left(-\pi \sin^{-1} X + c_2\right)\,, & \text{if } d_2 \le X \le 1\,, \\ \left(b_1 \sin^{-1} X + b_2\right)\,, & \text{if } d_1 \le X \le d_2\,, \\ c_1\,, & \text{if } 0 \le X \le d_1\,, \end{cases} \tag{23}$$

where $c_1$, $c_2$, $b_1$ and $b_2$ are given in terms of $d_1$ and $d_2$ by

$$\begin{aligned} c_1 &= -d_1^2 - \left(\sin^{-1} d_1\right)^2\,, \quad b_1 = \frac{\left(\sin^{-1} d_1\right)^2 - \left(\sin^{-1} d_2\right)^2 + d_1^2 - d_2^2}{\sin^{-1} d_2 - \sin^{-1} d_1}\,, \\ c_2 &= -d_2^2 + \pi \sin^{-1} d_2 - \left(\sin^{-1} d_2\right)^2\,, \quad b_2 = -b_1 \sin^{-1} d_1 - d_1^2 - \left(\sin^{-1} d_1\right)^2\,. \end{aligned} \tag{24}$$

The average MFPT, defined in (22), is determined in terms of $d_1$ and $d_2$ as

$$\overline{u}_0(d_1, d_2) \sim -\frac{1}{\pi D \delta^2}\left[J_0 + \mathcal{H}(d_1, d_2)\right]\,, \tag{25}$$

where the two integrals $J_0$ and $\mathcal{H}(d_1, d_2)$ are given by

$$J_0 \equiv \int_0^1 F(X)\left[\left(\sin^{-1}X\right)^2 + X^2 - \pi\sin^{-1}(X)\right]\,dX \approx -0.703\,,$$
$$\mathcal{H}(d_1,d_2) \equiv c_2\int_{d_2}^1 F(X)\,dX + \int_{d_1}^{d_2} F(X)\,\left((b_1+\pi)\sin^{-1}(X)+b_2\right)\,dX \qquad (26)$$
$$+\pi\int_0^{d_1} F(X)\,\left(\pi\sin^{-1}(X)+c_1\right)\,dX\,.$$

To minimize $\overline{u}_0$, we use a grid search to maximize the function $\mathcal{H}(d_1,d_2)$ on $0<d_1<d_2<1$. As derived in [11], this yields $d_{1\text{opt}}\approx 0.215$ and $d_{2\text{opt}}\approx 0.656$. In this way, and in terms of the original variables, the thin domain asymptotics predicts that the optimal trap locations and the optimal average MFPT have the scaling law

$$x_{1\text{opt}} \sim \frac{0.215}{b}\,,\quad x_{2\text{opt}} \sim \frac{0.656}{b}\,,\quad \overline{u}_{0\text{min}} \equiv \overline{u}_0(d_{1\text{opt}},d_{2\text{opt}}) \sim \frac{0.0179}{b^2 D}\,, \qquad (27)$$

for $b \ll 1$. In Fig. 6 (left) (reproduced from Fig. 12 of [11]) we observe that the scaling laws for the optimal distances on $b<0.5$ almost exactly reproduce results obtained from the CPM computed from the PDE (1) and from the hybrid asymptotic-numerical theory based on the LAS (8). From Fig. 6 (right), we observe that the scaling law for the optimal average MFPT closely approximates that from the CPM and the LAS (8) only when $b \le 0.25$.

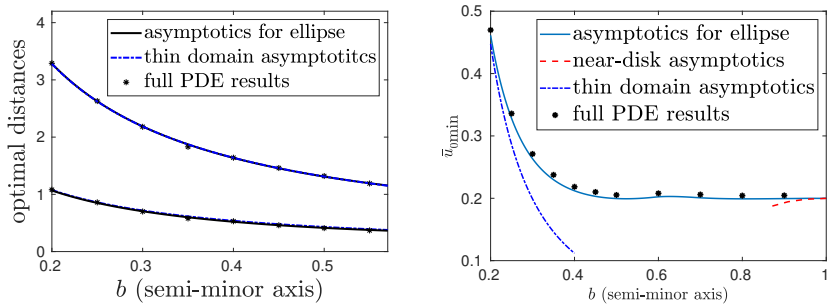


Fig. 6: Left: Optimal distances from the origin for a colinear four-trap pattern on the major-axis of an ellipse of area $\pi$ and semi-minor axis $b$. When $b \le 0.57$ the optimal pattern has two pairs of traps symmetrically located on either side of the origin. Right: optimal average MFPT $\overline{u}_{0\text{min}}$ versus $b$. Solid curves: optimal results from the LAS (8). Discrete points: full PDE results for (1) computed from the CPM. Dashed-dotted: thin-domain asymptotics (27). Dashed: near-disk results of [11].

For $N \le 50$, in [20] optimum trap configurations and the optimum average MFPT were computed numerically from a particle swarm optimization of the LAS (8) for various domain eccentricities $\kappa = \sqrt{1-(b/a)^2}$, where $b = 1/a$. In Fig. 7 (left) we

plot the discrete energy $q(\mathbf{x}_1, \ldots, \mathbf{x}_N)$ in (8) versus $N$ for $\kappa = 0$, 0.472, 0.802, and 0.995. Interestingly, we observe that as $N$ increases, the optimal $q$ seems to approach a universal curve that is independent of $\kappa$. In Fig. 7 (right) we show the computed optimal trap configurations when $\kappa = 0.802$ and $\kappa = 0.995$.

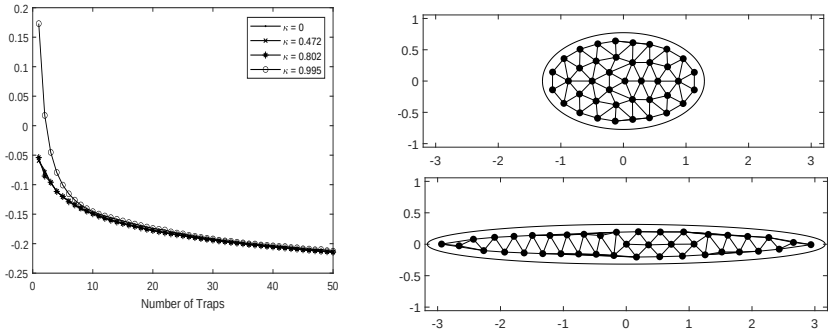


Fig. 7: Left: For an ellipse of area $\pi$, the optimal values of the discrete energy $q(\mathbf{x}_1, \ldots, \mathbf{x}_N)$ in (8) are plotted versus the number $N$ of traps for a few ellipse eccentricities $\kappa$. Right: optimal trap pattern for $N = 40$ when $\kappa = 0.802$ (top) and $\kappa = 0.995$ (bottom). The Delaunay triangulations are shown.

## 2.3 Periodic Trap Arrangements

Next we consider, as in [28], a periodic arrangement of traps, where the traps are centered at the lattice points of a Bravais lattice

$$\Lambda \equiv \left\{ m\boldsymbol{l}_1 + n\boldsymbol{l}_2 \,\middle|\, m,\, n \in \mathbb{Z} \right\}. \tag{28}$$

The *Wigner-Seitz (WS)* cell centered at a fixed $\boldsymbol{l} \in \Lambda$ is the set of all points that are closer to $\boldsymbol{l}$ than to any other lattice point. The fundamental WS cell $\Omega$ is the one centered at the origin. We assume that traps of a common shape with radius $O(\varepsilon) \ll 1$, as characterized by the logarithmic capacitance $d$ (5), are centered at each lattice point. The WS cells for an oblique lattice with circular traps are shown in Fig. 8.

Fixing the area $|\boldsymbol{l}_1 \times \boldsymbol{l}_2|$ of the WS cells to unity, and formulating the MFPT PDE in the fundamental WS cell, we seek to determine the specific Bravais lattice that minimizes the average MFPT for

$$D\triangle u = -1\,, \quad \mathbf{x} \in \Omega\backslash\Omega_\varepsilon\,; \quad u \in \mathcal{P}\,, \quad \mathbf{x} \in \partial\Omega\,; \quad u = 0\,, \quad \mathbf{x} \in \partial\Omega_\varepsilon\,, \tag{29}$$

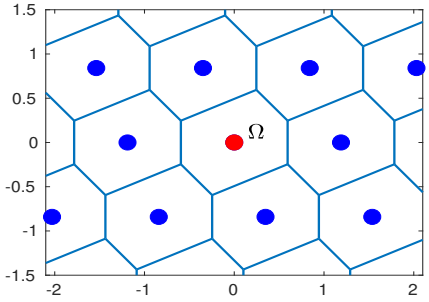


**Fig. 8** Wigner Seitz (WS) cells for an oblique Bravais lattice with generators $\boldsymbol{l}_1 = \left(2^{1/4}, 0\right)^T$ and $\boldsymbol{l}_2 = 2^{-1/4}\,(1,1)^T$ with circular traps (blue dots) of a common radius $\varepsilon$. The fundamental WS cell $\Omega$ of unit area is centered at the origin and contains the red trap.

where the operator $\mathcal{P}$ denotes periodic boundary conditions on $\partial\Omega$.

The asymptotic analysis needed to analyze (29) is analogous to that done in (4)–(8), except that now we must use the periodic source-neutral Green's function $G_p(\mathbf{x})$, defined by

$$\begin{aligned} \Delta G_p = \frac{1}{|\Omega|} - \delta(\mathbf{x})\,, \quad \mathbf{x}\in\Omega\,; \quad G_b \in \mathcal{P}\,, \quad \mathbf{x}\in\partial\Omega\,; \quad \int_\Omega G_p\, d\mathbf{x} = 0\,, \\ G_p \sim -\frac{1}{2\pi}\log|\mathbf{x}| + R_p + \frac{|\mathbf{x}|^2}{4} + o(|\mathbf{x}|^2)\,, \quad \text{as} \quad \mathbf{x}\to\mathbf{0}\,, \end{aligned} \tag{30}$$

instead of the Neumann Green's function. Setting $N = 1$ and $|\Omega| = 1$ in (8), we obtain in terms of $R_p$ and the logarithmic capacitance $d$ of the trap that

$$\overline{u}_0 \sim \frac{1}{2\pi D}\left(-\log[\varepsilon d]\right) + \frac{R_p}{D}\,, \quad \text{as} \quad \varepsilon\to 0\,. \tag{31}$$

In [31] a formula for the regular part $R_p$ was derived. By identifying a point $\mathbf{x}$ as a complex number $z = x + iy$ and by writing the Bravais lattice using the generators $\alpha\in\mathbb{C}$ and $\beta\in\mathbb{C}$ as $\Lambda \equiv \left\{ m\alpha + n\beta \,\middle|\, m,\, n\in\mathbb{Z}\right\}$, with $\mathrm{Im}(\beta/\alpha) > 0$ and $\mathrm{Im}(\bar{\alpha}\beta) = 1$ to fix $|\Omega| = 1$, it was derived in [31] that, with $\zeta \equiv \beta/\alpha$ and $e(w) \equiv e^{2\pi i w}$,

$$R_p = -\frac{1}{2\pi}\log(2\pi) - \frac{1}{2\pi}\log\left|\sqrt{\mathrm{Im}(\zeta)}\, e\left(\frac{\zeta}{12}\right)\prod_{n=1}^{\infty}\left(1-e(n\zeta)\right)^2\right|. \tag{32}$$

For a Bravais lattice with $|\Omega| = 1$, Theorem 2 of [31] proved that $R_p$ in (32) is minimized for a regular hexagonal lattice. From (31), this establishes that for Bravais lattices, the average MFPT as $\varepsilon\to 0$ is smallest for the hexagonal lattice. A plot of $R_p$ is shown in Fig. 9 for the one-parameter family of lattices $\Lambda$ with $\alpha = 1/\sqrt{\sin\theta}$ and $\beta = \alpha e^{i\theta}$. For the hexagonal and square lattices, where $\theta = \pi/3$ and $\theta = \pi/2$, we calculate $R_p \approx -0.210262$ and $R_{p0} \approx -0.208578$, respectively. From Fig. 9 we observe that $R_{p0}$ varies only slightly on the range $\theta > \pi/4$. As a result, the average MFPT is rather insensitive to the choice of lattice when $\theta > \pi/4$.

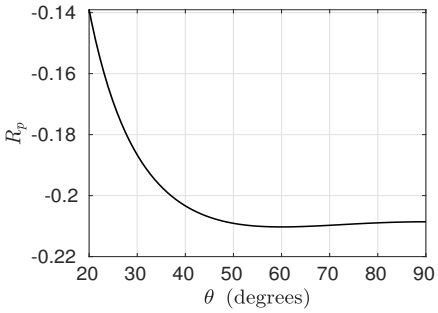


**Fig. 9** Plot of $R_p$ in (32) for oblique lattices with unit area of the primitive cell for which $\boldsymbol{l}_1 = (1/\sqrt{\sin(\theta)}, 0)^T$ and $\boldsymbol{l}_2 = (\cos(\theta)/\sqrt{\sin(\theta)}, \sqrt{\sin(\theta)})^T$. This yields $\alpha = 1/\sqrt{\sin\theta}$ and $\beta = \alpha e^{i\theta}$ in (32). The minimum occurs for the hexagon where $\theta = \pi/3$.

In [28], a higher order approximation for $\overline{u}_0$ was derived for a circular trap by using the fact that, since $\Omega$ has two lines of symmetry that intersect at the origin, the usual gradient term $\nabla_{\mathbf{x}} G_p|_{\mathbf{x}=\mathbf{0}} \cdot \mathbf{x}$ is absent in the local behaviour of $G_p$ in (30) as $\mathbf{x} \to \mathbf{0}$. From Principal Result 4.1 of [28], for the special case where $\Omega_\varepsilon$ is a circular disk of radius $\varepsilon$ the following improved asymptotic approximation was derived:

$$\overline{u}_0 \sim \frac{1}{2\pi D}\left(-\log\varepsilon\right) + \frac{R_p}{D} + \frac{\varepsilon^2}{D}\left[-\frac{1}{2}\log\varepsilon + \pi R_p + \frac{1}{2}\right] + o(\varepsilon^2)\,, \quad \text{as} \quad \varepsilon \to 0\,. \tag{33}$$

For a square or hexagonal lattice, for which $R_p$ was evaluated above, (33) yields

$$\begin{aligned} \overline{u}_0 &\sim \frac{-1}{2\pi D}\left(\log\varepsilon + 1.310533\right) - \frac{\varepsilon^2}{D}\left(\frac{1}{2}\log\varepsilon + 0.155266\right), \quad \text{(square)} \\ \overline{u}_0 &\sim \frac{-1}{2\pi D}\left(\log\varepsilon + 1.321117\right) - \frac{\varepsilon^2}{D}\left(\frac{1}{2}\log\varepsilon + 0.160559\right), \quad \text{(hexagon)}\,. \end{aligned} \tag{34}$$

We remark that the leading order result for the square lattice, without the $O(\varepsilon^2)$ correction, was derived previously in [32] by using the method of pseudo-potentials together with a numerical evaluation of certain lattice sums.

## 3 3-D Domains

For a bounded 3-D domain containing $N$ small traps, strong localized perturbation theory was used in [33] to approximate $\overline{u}_0$ in (3) for the MFPT-PDE (1). Related results for the MFPT and the splitting probability were derived in [34] using the method of pseudo-potentials. An extension of this narrow capture analysis has been developed recently in [35] and [36] to calculate the MFPT, the splitting probability, and conditional moments of the first passage time distribution in terms of the solution to a single modified narrow capture PDE in a 3-D and 2-D setting, respectively.

Focusing on the MFPT, for the 3-D narrow capture problem we obtain, in place of (5), that the local problem defined in the near-field region of a trap is to solve

$$\Delta_{\mathbf{y}} v = 0\,, \quad \mathbf{y} \notin \Omega_j\,; \quad v = 0\,, \quad \mathbf{y} \in \partial\Omega_j\,; \quad v \sim \frac{C_j}{|\mathbf{y}|} + O(|\mathbf{y}|^{-2}) + \cdots \text{ as } |\mathbf{y}| \to \infty\,. \tag{35}$$

Here $C_j$ is the capacitance of the trap and $\Omega_j = \Omega_{\varepsilon j}/\varepsilon$. The capacitance has two key properties: it is invariant under rotations of the trap shape and, over all trap shapes $\Omega_j$ of the same volume, $C_j$ is minimized for a spherical trap. The capacitance is known analytically for some simple trap shapes (see Table 1 of [33]).

For the 3-D problem, the Neumann Green's function $G(\mathbf{x};\mathbf{x}_j)$ is defined by

$$\begin{aligned} &\Delta G = \frac{1}{|\Omega|} - \delta(\mathbf{x}-\mathbf{x}_j)\,, \quad \mathbf{x}\in\Omega\,; \quad \partial_n G = 0\,, \ \ \mathbf{x}\in\partial\Omega\,; \quad \int_\Omega G\,d\mathbf{x} = 0\,, \\ &G \sim \frac{1}{4\pi|\mathbf{x}-\mathbf{x}_j|} + R_j + \nabla_{\mathbf{x}} R_j\cdot(\mathbf{x}-\mathbf{x}_j) + \cdots\,, \quad \text{as} \quad \mathbf{x}\to\mathbf{x}_j\,, \end{aligned} \tag{36}$$

where $R_j \equiv R(\mathbf{x}_j)$ is the regular part of the Green's function at $\mathbf{x} = \mathbf{x}_j$.

As derived in Principal Result 3.1 of [33], the average MFPT $\overline{u}_0$ for $\varepsilon \to 0$ is

$$\overline{u}_0 \sim \frac{|\Omega|}{D}\left(\frac{1}{4\pi\varepsilon N\bar{C}} + \frac{1}{N^2}p_c(\mathbf{x}_1,\ldots,\mathbf{x}_N) + O(\varepsilon)\right), \quad \text{where} \quad p_c \equiv \frac{\mathbf{C}^T\mathcal{G}\mathbf{C}}{(\bar{C})^2}\,. \tag{37}$$

Here $\mathbf{C} \equiv (C_1,\ldots,C_N)^T$, $\bar{C} \equiv N^{-1}(C_1 + \ldots C_N)$, and $\mathcal{G}$ is the Neumann Green's matrix in (9) now given in terms of the 3-D Green's function (36). For identically-shaped traps with a common capacitance $C = C_j$, for $j = 1,\ldots,N$, (37) becomes

$$\overline{u}_0 \sim \frac{|\Omega|}{D}\left[\frac{1}{4\pi\varepsilon NC} + \frac{1}{N^2}p(\mathbf{x}_1,\ldots,\mathbf{x}_N) + O(\varepsilon)\right], \quad \text{where} \quad p \equiv \mathbf{e}^T\mathcal{G}\mathbf{e}\,, \tag{38}$$

with $\mathbf{e} \equiv (1,\ldots,1)^T$. As a result, for $N$ identical traps, to minimize the average MFPT in (38), we must determine the global minimum of the discrete energy $p(\mathbf{x}_1,\ldots,\mathbf{x}_N)$.

For the unit sphere, we can evaluate the Neumann Green's matrix by using an analytical result for the 3-D Neumann Green's function and its regular part (see [33])

$$\begin{aligned} G(\mathbf{x};\mathbf{x}_j) &= \frac{1}{4\pi|\mathbf{x}-\mathbf{x}_j|} + \frac{1}{4\pi|\mathbf{x}||\mathbf{x}'-\mathbf{x}_j|} + \frac{1}{4\pi}\log\left(\frac{2}{1-\mathbf{x}\cdot\mathbf{x}_j + |\mathbf{x}||\mathbf{x}'-\mathbf{x}_j|}\right) \\ &\quad + \frac{1}{6|\Omega|}\left(|\mathbf{x}|^2 + |\mathbf{x}_j|^2\right) - \frac{7}{10\pi}\,, \\ R(\mathbf{x}_j) &= \frac{1}{4\pi\left(1-|\mathbf{x}_j|^2\right)} + \frac{1}{4\pi}\log\left(\frac{1}{1-|\mathbf{x}_j|^2}\right) + \frac{|\mathbf{x}_j|^2}{4\pi} - \frac{7}{10\pi}\,, \end{aligned} \tag{39}$$

where $|\Omega| = 4\pi/3$ and $\mathbf{x}' = \mathbf{x}/|\mathbf{x}|^2$ is the image point to $\mathbf{x}$ outside the unit sphere. With the Neumann Green's matrix easily calculated, a particle swarm optimizer can be used to optimize $\overline{u}_0$ from the discrete energies in (38) and (37).

For $N \le 20$ in [33] it was shown that the optimal trap locations lie, approximately, on a concentric shell inside the unit sphere, with possibly a center trap. The optimal

trap patterns for $N \leq 100$ identical traps and the optimal average MFPT were computed numerically in [37] by optimizing the discrete energy $p$ in (38).

## 4 Neumann Eigenvalue Problem for Laplacian

The problem of minimizing the average MFPT is closely related to the problem of identifying the trap configuration that maximizes the lowest, or fundamental, eigenvalue $\lambda_0$ of

$$\begin{aligned} &\Delta u + \lambda u = 0\,, \quad x \in \Omega \setminus \cup_{j=1}^{N} \Omega_{\varepsilon j}\,; \qquad \partial_n u = 0\,, \quad x \in \partial\Omega\,, \\ &\qquad u = 0\,, \quad x \in \partial\Omega_{\varepsilon j}\,, \quad j = 1, \ldots, N\,. \end{aligned} \tag{40}$$

When $\Omega$ is a 2-D bounded domain that contains traps of a common shape, it was shown in [17] that $\lambda_0 \ll 1$ is the smallest positive root of

$$\mathcal{F}(\lambda) = 0\,, \qquad \text{where} \qquad \mathcal{F}(\lambda) \equiv \det\left(I + 2\pi\nu\mathcal{G}_H\right)\,. \tag{41}$$

Here $\nu = -1/\log(\varepsilon d)$, $d$ is the logarithmic capacitance of the identical traps, and $\mathcal{G}_H$ is the $N \times N$ Helmholtz Green's matrix with matrix entries

$$(\mathcal{G})_{Hjj} = R_{Hj} \qquad \text{and} \quad (\mathcal{G})_{Hij} = (\mathcal{G})_{Hji} = G_H(\mathbf{x}_i; \mathbf{x}_j) \ \text{ for } \ i \neq j\,, \tag{42}$$

where $G_H(\mathbf{x}; \mathbf{x}_j)$ and its regular part $R_{Hj}$ satisfy

$$\begin{aligned} &\Delta G_H + \lambda G_H = -\delta(\mathbf{x} - \mathbf{x}_j)\,, \quad \mathbf{x} \in \Omega\,; \qquad \partial_n G_H = 0\,, \ \ \mathbf{x} \in \partial\Omega\,; \\ &G_H \sim -\frac{1}{2\pi}\log|\mathbf{x} - \mathbf{x}_j| + R_{Hj} + o(1)\,, \quad \text{as} \quad \mathbf{x} \to \mathbf{x}_j\,. \end{aligned} \tag{43}$$

By expanding $G_H$ for $\lambda \ll 1$ and substituting the resulting expression into (41), it was shown in Appendix C of [11] that

$$\lambda_0 \sim \frac{2\pi N\nu}{|\Omega|} - \frac{4\pi^2\nu^2}{|\Omega|}p(\mathbf{x}_1, \ldots, \mathbf{x}_N) + O(\nu^3)\,, \quad \text{with} \quad p(\mathbf{x}_1, \ldots, \mathbf{x}_N) \equiv \mathbf{e}^T\mathcal{G}\mathbf{e}\,, \tag{44}$$

where $\mathbf{e} \equiv (1, \ldots, 1)^T$ and $\mathcal{G}$ is the Neumann Green's matrix. For an arbitrary bounded 2-D domain, it follows by comparing (44) with (10) that, up to terms of $O(\nu^2)$, the trap locations that maximize the rate at which a Brownian particle is captured provide the minimizing trap configuration for the average MFPT.

A similar correspondence between the average MFPT and the fundamental Neumann eigenvalue holds for a bounded 3-D domain. For a configuration of $N$ traps centered at $\mathbf{x}_j \in \Omega$ with capacitances $C_j$ for $j = 1, \ldots, N$, it was shown in [33] that

$$\lambda_0 \sim \frac{4\pi\varepsilon N}{|\Omega|}\bar{C} - \frac{16\pi^2\varepsilon^2}{|\Omega|}p_c(\mathbf{x}_1, \ldots, \mathbf{x}_N) + O(\varepsilon^3)\,, \quad \text{where} \quad p_c \equiv \mathbf{C}^t\mathcal{G}\mathbf{C}\,. \tag{45}$$

Here $\bar{C} \equiv N^{-1}(C_1 + \ldots + C_N)$, $\mathbf{C} \equiv (C_1, \ldots, C_N)^T$, and $\mathcal{G}$ is the 3-D Neumann Green's matrix. By comparing (45) with (37) we conclude that, for $\varepsilon \to 0$, the trap locations that minimize the average MFPT also maximize $\lambda_0$.

## 5 Discussion and Open Challenges

We have surveyed some previous results for the optimization of the average MFPT for various narrow capture problems in a 2-D or 3-D domain. In the limit of small trap radii, we have shown that these optimization problems typically involve minimizing certain discrete energies for interacting particle systems, which are encoded by Green's matrices. These discrete energies that are derived from the strong localized perturbation analysis of the MFPT PDE are all closely related to the classical Fekete point energies [38, 39] of interacting Coulombic particle systems. When the Green's matrix can be calculated either explicitly or as a rapidly converging infinite series, a particle swarm optimizer can be readily used on the discrete energies to numerically determine the optimal trap set for a moderately small number of traps.

Our brief survey has focused on narrow capture problems with interior traps. Related narrow escape problems where the traps are located on the boundary of a domain have been analyzed for 2-D domains in [27, 40, 41] and for the sphere in [42] (see also the references therein). For the narrow escape problem from a sphere, optimal boundary trap configurations together with a scaling law have been computed in [43] and [12] from minimizing the appropriate discrete energy, which is defined in terms of an explicit analytical formula for the surface Neumann Green's function. A survey of results for the narrow escape problem is given in [4].

A related narrow capture problem is the Berg-Purcell [44] problem that involves calculating the effective capacitance and effective trapping rate of a sphere that has a large number $N$ of small nanotraps on its otherwise reflecting boundary. Strong localized perturbation theory has been used to derive a discrete energy, involving the exterior surface Neumann Green's function, that determines the effective capacitance [45, 46]. For equally-distributed points, and in the limit $N \to \infty$, a scaling law for the discrete energy has been used to derive an explicit formula for the effective trapping rate in the dilute trap fraction limit that improves upon the heuristic Berg-Purcell formula. This "first principles" result for the homogenized trapping rate has a similar form to some empirically postulated trapping rates used in [47] and [48]. Related work that determines the effective trapping rate for a simple model of semi-permeable traps is given in [49] and [50]. More biologically elaborate boundary trapping models that include the effect of patchy particles and or finite receptor kinetics have been analyzed recently in [51–53]. Based on an integral equation formulation of the relevant PDE, a fast full numerical solver for narrow capture and narrow escape problems in the sphere, which can effectively treat 2000 or more nanotraps, has been developed in [54].

Various extensions of the narrow capture modeling framework discussed in this survey can be incorporated into our hybrid asymptotic-numerical theory. For a col-

lection of traps that are only partially absorbing, we need only replace the boundary condition $v = 0$ on each trap by the Robin condition $\partial_n v + bv = 0$. From a numerical boundary integral solver on the local problems (5) and (35), the constants $d_j(b)$ and $C_j(b)$ can be computed for the 2-D and 3-D cases, respectively. A corresponding modified discrete energy can then be readily derived and optimized.

As a further extension of the methodology, in the 2-D case it was shown in [28] how to use a complex variable approach together with a least squares fitting to numerically calculate the logarithmic capacitance for a cluster of non-overlapping traps that are centered at some point in $\Omega$. Such trap clusters are characterized by inter-trap separations of $O(\varepsilon)$ in a confining domain of radius $O(1)$.

The numerical treatment for problems involving clusters of traps is closely related to the challenging problem of calculating the MFPT in the non-perturbative setting where the traps do not have asymptotically small radii. In this context, an exact solution involving bipolar coordinates was found in [55] for calculating the MFPT in a circular domain containing one non-concentric disk of arbitrary radius. For a spherical domain containing non-overlapping spheres of arbitrary radii, a semi-analytical method based on the generalized method of separation of variables (GMSV) was developed in [56] to calculate the Green's function for the Laplacian in the perforated domain. In this approach, the global approximate solution is represented as a linear combination of local solutions involving solid harmonics centered near at each inclusion. Translation addition theorems for solid harmonics are then used for deriving a linear algebraic system that allows all the boundary conditions to be satisfied. This semi-analytical approximation of the Green's function is key for estimating various stationary quantities such as the escape probability, harmonic measure, and the MFPT. This GMSV approach of [56] should be ideal for estimating the capacitance of a cluster of non-overlapping spherical traps in $\mathbb{R}^3$. For the same class of domains, an extension of this GMSV methodology was developed in [57] to approximate the Green's function for the reduced-wave equation. This Green's function arises in calculating the Laplace transform for the time-dependent probability distribution.

We now discuss a few open problems related to narrow capture problems.

To easily implement a particle swarm optimizer on the discrete energy associated with the Neumann Green's matrix it is essential to efficiently calculate the Neumann Green's function and its regular part. For the 2-D case, this can be done for a disk, for a rectangle [26, 27], and for an ellipse. For 3-D domains, the Neumann Green's function can be readily calculated for a sphere. For a triclinic cell in 3-D, the source neutral periodic Green's function can be evaluated in terms of rapidly converging infinite series [58]. For arbitrary 2-D or 3-D domains, a key open problem is to develop a fast multipole algorithm, such as done in [59] for the reduced-wave equation, to rapidly calculate the Neumann Green's function and its regular part for (7) and (36). By using such a fast numerical evaluation of the Neumann Green's matrix, it should be numerically tractable to use a particle swarm optimizer on either the LAS (8) for the 2-D domain or on (37) for a 3-D domain so as to numerically identify optimal trap configurations.

For 2-D or 3-D domains with a collection of interior traps, it would be interesting to derive an approximate scaling law for the optimal average MFPT when $N \to \infty$.

Intuitively, one might expect that the optimal trap configuration for large $N$ has a near lattice structure in the interior of the domain with only a small modification needed near the domain boundary. It would be interesting to investigate this conjecture and to relate the large $N$ limiting problem, but with $N\sum_j |\Omega_{\varepsilon j}| \ll 1$, to results that can be derived by homogenization theory in the dilute trap fraction limit.

Another open problem is to determine the optimal lattice arrangement for a 3-D periodic lattice with identical shaped traps centered at the lattice points. The main challenge here is to provide a tractable analytical formula for the regular part of the periodic source-neutral Green's function for the 14 distinct Bravais lattices.

Finally, it would also be worthwhile to investigate optimizing MFPT problems for some highly challenging situations where the traps are not stationary, such as in [60], in §4.3 of [7], and in [61]. In particular, the optimal distance from the origin for a trap that rotates with a given angular velocity on a ring concentric within the unit disk was shown in [60] to have a highly intricate bifurcation structure.

**Acknowledgements** We gratefully acknowledge the contributions of our collaborators, Andrew Bernoff, Jason Gilbert, Sarafa Iyaniwura, Theodore Kolokolnikov, Alan Lindsay, Colin MacDonald, Wesley Ridgway, Michele Titcombe, and Tony Wong to some of the work described herein.

## References

1. O. Bénichou, R. Voituriez, From first-passage times of random walks in confinement to geometry-controlled kinetics, Physics Reports. **539**, 225–284, (2014).
2. D. Holcman, Z. Schuss, Time scale of diffusion in molecular and cellular biology, J. of Physics A: Math. and Theor. **47**, 173001, (2014).
3. J. Yang, I. Kupka, Z. Schuss, D. Holcman, Search for a small egg by spermatozoa in restricted geometries, J. Math. Biol. **73**, 948–964, (2016).
4. D. Holcman, Z. Schuss, The Narrow Escape Problem, SIAM Review. **56**, 213–257, (2014).
5. S. Redner, *A Guide to First-Passage Processes*, (Cambridge University Press, Cambridge, 2001).
6. R. Metzler, G. Oshanin, S. Redner, eds., *First-passage phenomena and their applications*, (World Scientific, Singapore, 2014).
7. S. Iyaniwura, T. Wong, M. J. Ward, C. Macdonald, Simulation and optimization of mean first passage time problems in 2-D using numerical embedded methods and perturbation theory, Multiscale Model. Simul. **19**, 1367–1393, (2021).
8. M. J. Ward, W. D. Henshaw, J. B. Keller, Summing logarithmic expansions for singularly perturbed eigenvalue problems, SIAM J. Appl. Math. **53**, 799–828, (1993).
9. M. J. Ward, J. B. Keller, Strong localized perturbations of eigenvalue problems, SIAM J. Appl. Math. **53**, 770–798, (1993).
10. M. J. Ward, Spots, traps, and patches: Asymptotic analysis of localized solutions to some linear and nonlinear diffusive systems, Nonlinearity **31**, R189, (2018).
11. S. Iyaniwura, T. Wong, C. B. Macdonald, M. J. Ward, Optimization of the mean first passage time in near-disk and elliptical domains in 2-D with small absorbing traps, SIAM Review **63**, 525–555, (2021).
12. W. J. M. Ridgway, A. Cheviakov, Locally and globally optimal configurations of N particles on the sphere with applications in the narrow escape and narrow capture problems, Phys. Rev. E., **100**, 042413, (2019).

13. A. Burchard, J. Denzler, On the geometry of optimal windows, with special focus on the square, SIAM J. Math. Anal. **37**, 1800–1827, (2006).
14. E. M. Harrell, P. Kröger, K. Kurata, On the placement of an obstacle or a well so as to optimize the fundamental eigenvalue, SIAM J. Math. Anal. **33**, 240–259, (2001).
15. A. Henrot, On minimization problems for eigenvalues of the Laplacian, J. Evol. Equat. **3**, 443–461, (2003).
16. J. Denzler, Windows of given area with minimal heat diffusion, Trans. Amer. Math. Soc. **351**, 569–580, (1999).
17. T. Kolokolnikov, M. S. Titcombe, M. J. Ward, Optimizing the fundamental Neumann eigenvalue for the Laplacian in a domain with small traps, Europ. J. Appl. Math. **16**, 161–200, (2005).
18. D. Coombs, R. Straube, M. J. Ward, Diffusion on a sphere with localized traps: Mean first passage time, eigenvalue asymptotics, and Fekete points, SIAM J. Appl. Math. **70**, 302–332, (2009).
19. F. Paquin-Lefebvre, S. Iyaniwura, M. J. Ward, Asymptotics of the principal eigenvalue of the Laplacian in 2-D periodic domains with small traps, Europ. J. Appl. Math. **33**, 646–673, (2021).
20. J. Gilbert, A. Cheviakov, Global optimization of the mean first passage time for narrow capture problems in elliptic domains, Europ. J. Appl. Math. **34**, 1269–1287, (2023).
21. Y. Chen, C. B. Macdonald, The closest point method and multigrid solvers for elliptic equations on surfaces, SIAM J. Sci. Comp. **37**, A134–A155, (2015).
22. V. Kurella, J. C. Tzou, D. Coombs, M. J. Ward, Asymptotic analysis of first passage time problems inspired by ecology, Bull. Math. Biol. **77**, 83–125, (2015).
23. A. Ismael, F. Vaz, L. N. Vicente, A particle swarm pattern search method for bound constrained global optimization, J. Global Optim. **39**, 197—219, (2007).
24. J. Currie, D. I. Wilson, N. Sahinidis, J. Pinto, OPTI: Lowering the barrier between open source optimizers and the industrial MATLAB user. Foundations of computer-aided process operations, **24** (2012).
25. J. Kennedy, Particle swarm optimization. Encyclopedia of machine learning, 760–766, (2010).
26. T. Kolokolnikov, M. J. Ward, J. Wei, Spot self-replication and dynamics for the Schnakenburg model in a two-dimensional domain, J. Nonl. Sci, **19**, 1–56, (2009).
27. S. Pillay, M. J. Ward, A. Peirce, T. Kolokolnikov, An asymptotic analysis of the mean first passage time for narrow escape problems: Part I: Two-dimensional domains, Multiscale Model. Simul. **8**, 803–835, (2010).
28. S. Iyaniwura, M. J. Ward, Asymptotic analysis for the mean first passage time in finite or spatially periodic 2-D domains with a cluster of small traps, ANZIAM J. **63**, 1–22, (2021).
29. D. S. Grebenkov, A. T. Skvortsov, Mean first-passage time to a small absorbing target in an elongated planar domains, New J. Phys. **22**, 113024, (2020).
30. D. S. Grebenkov, A. T. Skvortsov, Mean first-passage time to a small absorbing target in three-dimensional elongated domains, Phys. Rev. E. **105**, 054107, (2022).
31. X. Chen, Y. Oshita, An application of the modular function in nonlocal variational problems, Arch. Rat. Mech. Anal. **186**, 109–137, (2007).
32. D. C. Torney, B. Goldstein, Rates of diffusion-limited reaction in periodic systems, J. Stat. Phys. **49**, 725–750, (1987).
33. A. Cheviakov, M. J. Ward, Optimizing the principal eigenvalue of the Laplacian in a sphere with interior traps, Math. and Comput. Model. **53**, 1394–1409, (2011).
34. S. Condamin, O. Bénichou, M. Moreau, Random walks and Brownian motion: A method of computation for first passage times and related quantities in confined geometries, Phys Rev. E. **75**, 021111, (2007).
35. P. C. Bressloff, Asymptotic analysis of target fluxes in the three-dimensional narrow capture problem, Multiscale Model. Simul. **19**, 612-–632, (2021).
36. P. C. Bressloff, Asymptotic analysis of extended two-dimensional narrow capture problems, Proc. Roy. Soc. A: Math. Phys. Eng. Sci. **477**, 20200771, (2021).
37. J. Gilbert, A. Cheviakov, Globally optimal volume-trap arrangements for the narrow-capture problem inside a unit sphere, Phys. Rev. E. **99**, 012109, (2019).

38. E. B. Saff, A. B. J. Kuijlaars, Distributing many points on a sphere, Math. Intelligencer **19**, 5–11, (1997).
39. E. A. Rakhamanov, E. B. Saff, Y. M. Zhou, Minimal discrete energy on the sphere, Math. Res. Lett. **1**, 647–662, (1994).
40. A. Singer, Z. Schuss, D. Holcman, Narrow escape, Part II: The circular disk, J. Stat. Phys. **122**, 465–489, (2006).
41. D. S. Grebenkov, Universal formula for the mean first passage time in planar domains, Phys. Rev. Lett. **117**, 260201, (2016).
42. A. F. Cheviakov, M. J. Ward, R. Straube, An asymptotic analysis of the mean first passage time for narrow escape problems: Part II: The sphere, Multiscale Model. Simul. **8**, 836–870, (2010).
43. A. Cheviakov, D. Zawada, Narrow-escape problem for the unit sphere: Homogenization limit, optimal arrangements of large number of traps, and the N2 conjecture, Phys. Rev. E. **87**, 042118, (2013).
44. H. C. Berg, E. M. Purcell, Physics of chemoreception. Biophys. J. **20**, 193–219, (1977).
45. A. E. Lindsay, A. J. Bernoff, M. J. Ward, First passage statistics for the capture of a Brownian particle by a structured spherical target with multiple surface traps, Multiscale Model. Simul. **15**, 74–109, (2017).
46. A. E. Lindsay, A. J. Bernoff, Numerical approximation of diffusive capture rates by planar and spherical surfaces with absorbing pores, SIAM J. Appl. Math. **78**, 266–290, (2018).
47. C. B. Muratov, S. Y. Shvartsman, Boundary homogenization for periodic arrays of absorbers, Multiscale Model. Simul. **7**, 44-61, (2008).
48. A. M. Berezhkovskii, M. I. Monine, C. B. Muratov, S. Y. Shvartsman, Homogenization of boundary conditions for surfaces with regular arrays of traps, J. Chem. Phys. **124**, 036103, (2006).
49. A. J. Bernoff, A. E. Lindsay, D. D. Schmidt, Boundary homogenization and capture time distributions of semi-permeable membranes with periodic patterns of reactive sites, Multiscale Model. Simul. **16**, 1411–1447, (2018).
50. A. E. Lindsay, A. N. Hernandez, B. Quaife, Trapping of planar Brownian motion: Full first passage time distributions by Kinetic Monte-Carlo, asymptotic and boundary integral methods, Multiscale Model. Simul. **20**, 1284–1314, (2022).
51. G. Handy, S. D. Lawley, Revising Berg-Purcell for finite receptor kinetics, Biophysical J., **120**, 2237–2248, (2021).
52. S. D. Lawley, Boundary homogenization for trapping patchy particles, Phys. Rev. E. **100**, 032601, (2019).
53. C. E. Plunkett, S. D. Lawley, Boundary homogenization for patchy surfaces trapping patchy particles, J. Chem. Phys. **158**, 094104, (2023).
54. J. Kaye, L. Greengard, A fast solver for the narrow capture and narrow escape problems in the sphere, J. Comput. Phys., **5**, 100047, (2020).
55. R. Stana, G. Lythe, C. Molina-Páris, Diffusion in a disk with inclusion, SIAM J. Appl. Math. **81**, 1287–1302, (2021).
56. D. S. Grebenkov, S. D. Traytak, Semi-analytical computation of Laplacian Green's functions in three-dimensional domains with disconnected spherical boundaries, J. Comput. Phys. **379**, 91–117, (2019).
57. D. S. Grebenkov, Diffusion toward non-overlapping partially reactive spherical traps: Fresh insights into classical problems, J. Chem. Phys. **152**, 244108, (2020).
58. S. Tyagi, Coulomb potentials in two and three dimensions under periodic boundary conditions, J. Chem. Phys. **122**, 014101, (2005).
59. M. C. Kropinski, B. D. Quaife, Fast integral equation methods for the modified Helmholtz equation, J. Comput. Phys. **230**, 425–434, (2011).
60. J. C. Tzou, T. Kolokolnikov, Mean first passage time for a small rotating trap inside a reflective disk, Multiscale Model. Simul. **13**, 231–255, (2015).
61. A. E. Lindsay, J. C. Tzou, T. Kolokolnikov, Optimization of first passage times by multiple cooperating mobile traps, Multiscale Model. Simul. **15**, 920–947, (2017).